Fluid Flow with Three Upstream Configurations in Freezing Tubes.

J. A. Whitehead

Physical Oceanography Department, Woods Hole Oceanographic Institution,

Corresponding author: J. A. Whitehead (jwhitehead@whoi.edu)

02 NOV 2020

Key Points

- Criteria are found for a simple model with liquid freeze-up versus flow-through in freezing tubes
- Upstream flows alter upstream pressures so that the freezing flow is modified
- Three examples of combining freezing with upstream dynamics are analyzed, compressible upstream, throttled upstream, and an upstream manifold

(The above elements should be on a title page)

Abstract

The flow and stability of liquid through a tube at subfreezing temperature can be modified by the upstream flow conditions. A simplified model for the dynamics is used to show behavior 3 different upstream configurations. When certain stability parameters are met: 1. A compressible reservoir has oscillatory behavior . 2. A tube fed by a constriction with a large upstream pressure behaves like a freezing faucet during winter. 3. Multiple tubes connected by an upstream manifold evolve to some selected flowing tubes and others seeping with their spacing inversely proportional to manifold flow resistance. Numerically, a minimum radius needs to be invoked in many cases to avoid excessive upstream pressure. Results have numerous applications such as wintertime ice formation at natural springs, the formation of magma tubes, spacing of volcanism, and the distance that liquid flows through freezing surroundings.

Plain Language Summary

The dynamics of viscous liquid flow in an upstream region must naturally be considered in conjunction with flow through a freezing region. This is because when liquid flows into a freezing region, the pressure change that arises from the accumulation of solid modifies the upstream pressure, which can in turn modify flow rates in both regions. This paper shows examples of three different upstream situations that produce feedback between upstream flow and the freezing region. The interaction leads to complicated results such as oscillations, intense flow channelization in subfreezing surroundings, and freeze-up of some portions of the downstream region. The fundamental nature of the interaction between upstream and freezing flows begins to explain the complicated nature of freezing flows in many areas of earth science.

1. Introduction

As liquid flows into a region with boundary temperature below the solidus temperature, the solid typically forms near the boundaries leaving one or more melted cores where liquid flows. With complicated regions, some of the cores might become tortuous or freeze shut progressively in time. Naturally the conditions separating flow and freeze-up depend upon the dimensions and geometry of the layout, the relative temperatures of the upstream fluid and the walls compared to the temperature of solidification and fluid properties (e. g. viscosity, thermal conductivity, and latent heat of solidification) (Mulligan and Jones 1976, Epstein and Chueng 1983, Richardson 1983, 1985, 1986, Kavanagh et al. 2018). A notable feature, to be expounded here using three configurations, is a dependence of the results upon the nature of the upstream conditions, (Figure 5 in Epstein and Chueng 1983, Holmes 2007, Holmes-Cerfon and Whitehead 2011 (called HCW here)).

Three configurations are used because numerous studies exist with little attention paid to the upstream conditions in engineering and earth sciences. In engineering these include injection molding, (Richardson 1983, 1985, 1986), freezing of water (Zerkle and Sunderland 1968, Mulligan and Jones 1976), ventilation (Hirata and Ishihara 1985, Weigand et al. 1997) and metallurgy (Chadam, et al. 1986, Daccord 1987). In Earth sciences, examples include the dynamics and stability of lava and magma tubes (Rubin 1993, Sakimoto and Zuber 1998, Dragoni et al. 2002, Sakimoto and Gregg 2001, Klingelhofer et al. 1999), glacier drainage, (Björnsson 1998), and magma fissure flows (Bruce and Huppert 1989, 1990).

If viscosity increases with colder temperature, liquid flowing into cold regions has similar behavior. For progressively larger viscosity contrast, flow becomes focused into narrow channels surrounded by cold sluggish flow. A similar dependence also exists upon the upstream conditions (Whitehead and Helfrich 1991, Helfrich 1995). Various geometries include regular circular slots, (Whitehead and Helfrich 1991, Helfrich, 1995, Wylie and Lister 1995, Wylie et al. 1999a), gelatin (Pansino et al. 2019 and citations therein) and cracks (Taisne and Tait 2011, Taisne, et al. 2011).

An upstream region might have many configurations. In engineering the injection can come from one or more pumps or from a reservoir at fixed pressure. In the earth, the source can be chambers, mushy zones, lakes or fluids squeezed out by high pressure regions. A personal witness of the interplay came from a lava outbreak that I watched in Hawaii. Each lobe of molten lava broke out and temporarily flowed only to gradually be retarded by an accumulating solidified crust. Meanwhile, the older upstream crust visibly inflated as flow resistance in the solidifying lobe increased. This greater upstream pressure ultimately ruptured crust at another location, producing an additional lobe. The result was a growing cluster of lobes that produced a complicated pattern of pahoehoe. The interplay of solidifying flow and upstream pressure was both clearly apparent and obviously complicated.

The manner in which the width of a channel of melt adjusts in sheet-flow as flow magnitude changes was first apparent to me observing an unpublished laboratory experiment using liquid flowing in a gap radially outward from the center of a carefully levelled aluminum disk painted black and kept at a temperature below the solidus. The gap (of fixed thickness) was between a transparent acrylic lid and the disk. The apparatus was similar to those for transient experiments with paraffin [*Whitehead and Helfrich*. 1991] and flow of oversaturated water [*Kelemen et al., 1994*], both of which demonstrated the formation of a channel. We used a positive displacement pump at a steady volume flux rate to provide a liquid with its temperature above the solidus into the center of the disk. Therefore, the liquid was forced to flow outward in the radial direction to the outer radius where it was cooled. Some of it solidified and the rest spilled into a catch basin.

A channel of flowing clear melt revealed the black bottom that increasingly became surrounded by white stagnant solid. For very small pumping rate, the evolution was complicated but it still ended with the formation of a tiny channel. After the pump was started, the flow channel terminated at a frozen fan of material, (Figure 1a) and then a new outbreak of flowing liquid would form to the left or the right (Figure 1b). This would make a second fan, which was followed by another outbreak. Then, there were many subsequent cycles of outbreak-fan formation (Figure 1c). In some cases the fans did not even extend to the outer radius of the disk before they were completely frozen. In other cases an air hole became surrounded with solid. However, the sequence of fan formation and outbreak ultimately spiraled around the entire 360^0 circle of the disk so that the total region ended up being filled with solid. At that point, flowing liquid was still present in a crescent shaped region near the center. The video (in supplementary materials) indicates that the liquid forced the lid upward a small amount and then flowed radially outward within a very thin gap between the solid and lid. This radial flow is almost completely axisymmetric, and it is always followed by the appearance of one rapidly amplified dark drainage channel (Figure 1d) extending from the central hole to the outside rim of the cylinder. The dark line becomes progressively darker and wider over about a five-minute period, during which we believe the channel melted its way through the wax down to the aluminum disk. Thereafter, the entire flow occupied this channel whose size remained fixed (Figure 1e). Some student projects were started in this way and this sequence always happened. Measurement showed that the width of the final channel is proportional to flux rate, (C. J. Mills, private communication).

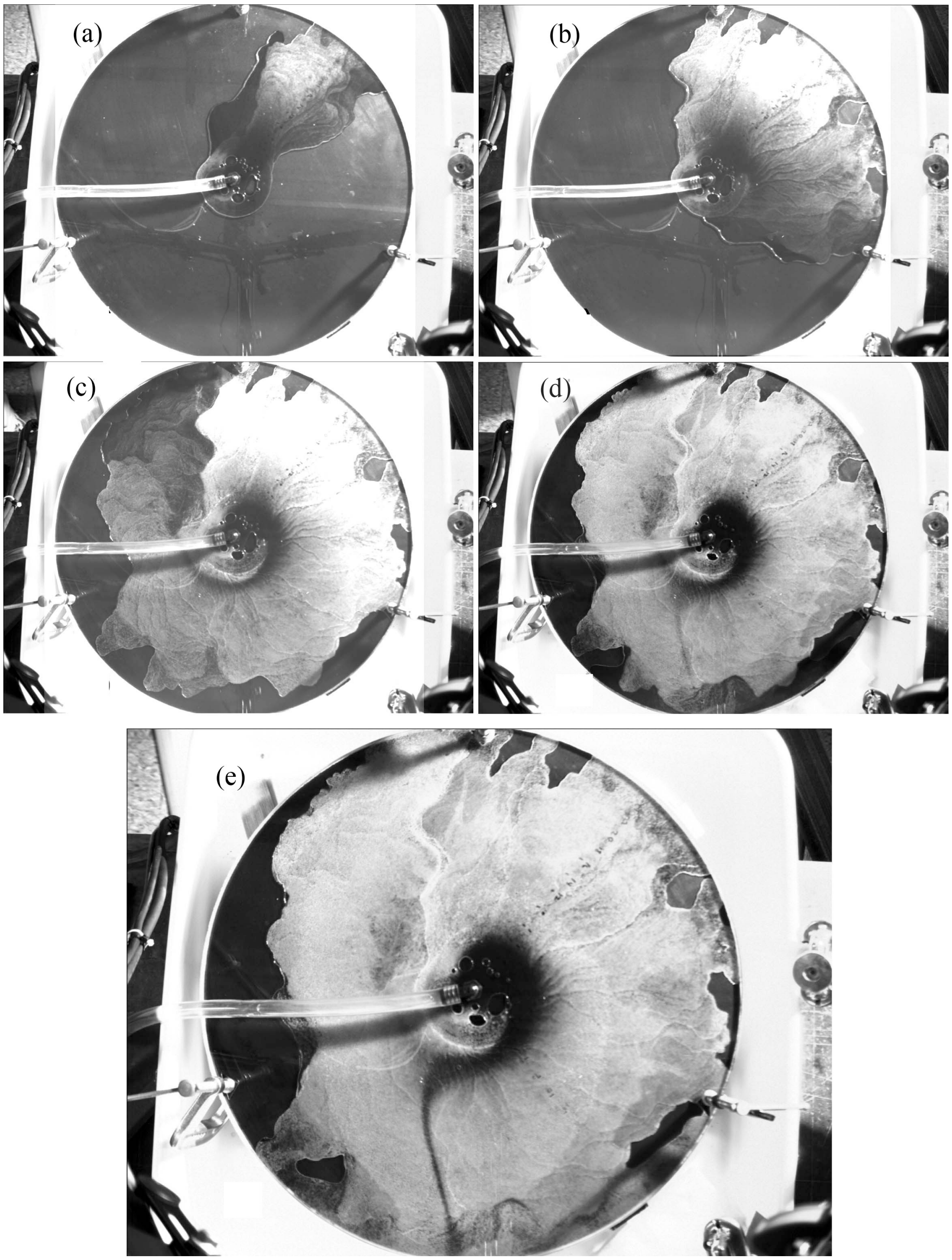

Figure 1. The evolution of a drainage tube at very small flow rate.

Here, the mathematical solution in HCW for flow through a freezing tube is replaced by a simple model with analytic functions. Section 2 reviews the HCW solution and develops the simple model. Section 3 analyzes the stability properties of this model with a compressible upstream condition as in HCW and then shows numerical calculations. Freeze-up with pressure approaching infinity causes some difficulty that is overcome by adopting a minimum radius, which generates seepage flow instead of complete freezing. This bends the pressure curve for slow flow down to zero at the origin. The resulting oscillations are like those with viscosity-temperature variation in the laboratory (Whitehead and Helfrich 1991). Section 4 presents a criterion for freeze-up of a dripping faucet in freezing weather and Section 5 analyzes flow and freeze-up for 2 up to 10^4 multiple tubes fed by a manifold. The calculations must include seepage flow and results produce a formula relating the spacing of active tubes to the parameter expressing the relative resistances of the active and manifold tubes divided by the upstream volume flux rate. Results are applied to some problems in igneous flow.

2. A freezing pipe flow

The three upstream situations are used along with a simplified model for the flow in the freezing region that comes from one of the simplest examples: a liquid flowing through a pipe held below the liquid solidus temperature developed by Zerkle and Sunderland (1968), and Sakimoto and Zuber (1998, and references therein). Solutions are based on separation of variables with eigenvalues and eigenfunctions by Graetz (1883). Holmes (2007) and subsequently HCW asserted that the central attribute that leads to instability of these flows is that pressure drop becomes infinite in the limits of zero and infinite flux rate. Therefore, there is a pressure drop minimum in the middle.

2.1 The solution

HCW's formulation is briefly reviewed (using some different symbols). Liquid enters one end of a pipe of radius r_0 and length L (x-direction) at temperature T_i, (Figure 2a,b). Pipe wall temperature T_0 is colder than the solidus temperature T_s that lies at radius $\alpha(x, t_d)$, where x is distance downstream and t_d is dimensional time. The coefficients for thermal conductivity, specific heat, density, viscosity and latent heat of fusion are all constant. Volume flux rate Q and pressure (P) gradient along the pipe is found by integrating the low Reynolds number Stokes flow equations over the radial coordinate *r* from the center to the solid surface

$$\frac{dP}{dx} = -\frac{8\mu Q}{\pi\alpha^4(x,t_d)} \tag{2.1.1}$$

where μ is fluid viscosity. Temperature field within the solid is called T_e and is assumed to evolve slowly enough for thermal conduction to be steady. For a small pipe aspect ratio, conduction along the pipe axis direction is neglected so

$$T_e = \frac{T_0 - T_s}{ln\frac{r_0}{\alpha(x,t_d\ )}} ln\frac{r}{\alpha(x,t_d)} + T_s \quad . \tag{2.1.2}$$

In the liquid, temperature *T* is advected along-stream and diffused across-stream.

$$u\frac{\partial T}{\partial x} = \frac{\kappa}{r}\frac{\partial}{\partial r}\left(r\frac{\partial T}{\partial r}\right), \tag{2.1.3}$$

where κ is thermal diffusivity. This has boundary conditions $T=T_s$ at $r=\alpha(x,t_d)$, $T=T_i$ at $r=x=0$, and $\frac{\partial T}{\partial r} = 0$ at $r=0$.

Last, the evolution of the solidus radius follows the Stefan equation at each value of *x*.

$$\frac{L_H}{C_p}\frac{\partial\alpha(x,t_d)}{\partial t_d} = \kappa\left(\frac{\partial T_e}{\partial r}\bigg|_{r=\alpha(x,t_d)} - \frac{\partial T}{\partial r}\bigg|_{r=\alpha(x,t_d)}\right), \tag{2.1.4}$$

where L_H is latent heat of fusion and C_p is specific heat of the liquid.

The non-dimensional forms are derived using $t_d = (r_0^2\, L_H/C_p\kappa(T_i - T_S))t$, $x = L\chi$, $\alpha = r_0 a(\chi,t)$, $\theta = (T - T_0)/(T_i - T_s)$, $\theta_e = (T_e - T_s)/(T_i - T_s)$, $Q = \frac{1}{2}\pi\kappa L q$, and $P = 4\mu\kappa L^2 p/r_0^4$ so

$$p(t) = q(t)\int_0^1 \frac{1}{a^4(\chi,t)}d\chi. \tag{2.1.5}$$

and (2.1.4) is

$$\frac{\partial a(\chi,t)}{\partial t} = \frac{1}{a(\chi,t)}[E(a(\chi,t)) - I(\chi,q(t))] \tag{2.1.6}$$

where the conductive heat flow from the solid-liquid interface toward the outer radius is

$$E\big(a(\chi,q,t)\big) = \frac{-T_n}{\ln a(\chi,q,t)}, \qquad (2.1.7)$$

and the conductive heat flow from the liquid onto the interface is $I(\chi,q)$. To calculate *I,* the solution for liquid temperature *T* uses the eigenvalues and eigenfunctions from Graetz (1883). The results are governed by the dimensionless temperature difference $T_n = (T_S - T_0)/(T_i - T_S)$ (this sign and the sign in front of the right hand side of (2.1.7) are opposite to HCW). The radius changes with the downstream distance (Figure 2c), and for steady flow, the scaling dictates that for given values of Q and κ the dimensional distance downstream from the origin scales like χ/q. This geometric independence from *Tn* means the 4 interface profiles in Figure 2c are all versions of the same curve.

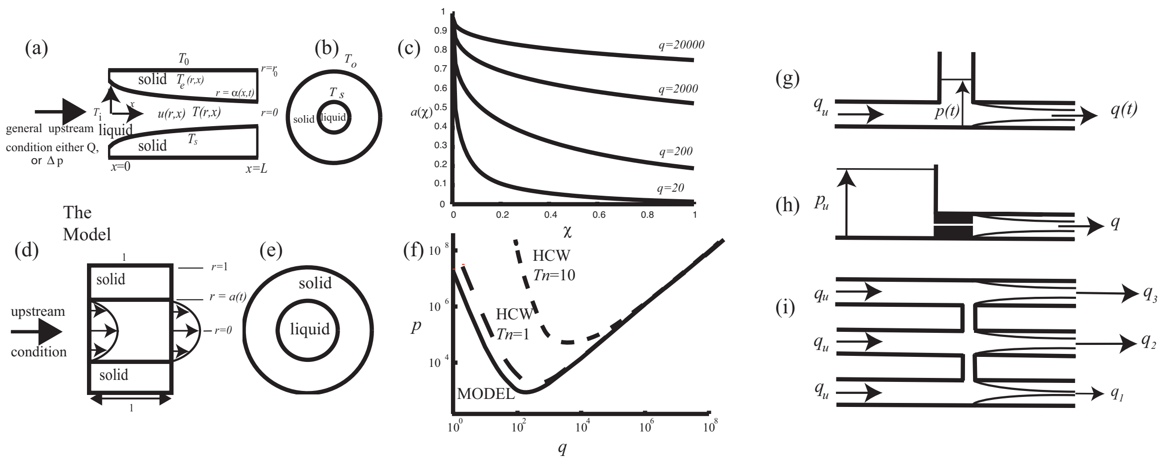

Figure 2. (a) A tube held at a temperature below the solidus with liquid flowing from left to right. The radius *α(x)* of the solid-liquid interface changes in the flow direction. (b) View into the axis. (c) Profiles of the dimensionless radius of liquid *a(χ)* along the tube for 4 different values of volume flux rate *q*. The curves are identical except that each is stretched differently in the lateral direction (From Holmes 2007). (d, e) Side and end views of the simplified model of the tube. (f) Pressure drop *p* through the tube as a function of flow rate *q* for two values of *Tn* (dashed curve), and the curve from this simplified model (heavy curve). (g) A compressible upstream, represented here by a reservoir in a field of gravity with a free surface fed by constant flux rate. (h) A fixed resistance in series with the tube fed at constant upstream pressure, represented here by an infinite upstream reservoir at fixed elevation in a field of gravity. (i) Multiple tubes connected with a manifold (top view). Each upstream location is fed by the same flux rate. Flow between each segment of the manifold has resistance coefficient *C*. This example shows a hypothetical situation with smaller flow rate in one tube.

The pressure drop across the tube is a function of volume flux rate q (shown by dashed lines in Figure 2f) that requires solving the eigenfunctions and eigenvalues of the problem. The solution has a minimum value p_{min} over the entire range, and p goes to infinity at q=0,∞.

2.2 The simplified model

It is convenient to use a simpler pressure-flux rate relationship than HCW but one with the same form (Figure 2f). This simplified model has a liquid-solid interface with constant radius $a(t)$ that does not change in the flow direction (Figure 2d,e).

The dimensionless form of (2.1.1) is simply

$$p = \frac{q}{a^4}. \tag{2.2.1}$$

The conductive heat flux relation along the tube into the solid $E(a(x), q, t)$ is replaced by one that does not vary along the flow direction. The dimensionless equivalent for the first term in a Taylor series expansion about ln(1-a) is $E(a) = -T_n/\,(1-a)$. This makes the heat flow equation analytically solvable. The relation is best for a close to 1 with the values changing significantly from (2.1.7) as $a \longrightarrow 0.2$. Therefore, the term $1/a(t)$ in front of E is also set to 1. The resulting formula governs heat flow in cartesian coordinates through a slab over the inside area of the tube at r =1. We set $l(\chi, q) = q/4$ in (2.1.6) so the model has the inflowing hot liquid deposit as much heat along the tube as possible and exit at the solidus temperature. These all are significant physical simplifications from the exact problem but they do express the physics of melt back and freeze forward with simple and useful relations. The radius evolution for the simplified model in Figure 2c,d is thereby substantially simplified to

$$\frac{da}{dt} = -\frac{T_n}{1-a} + \frac{q}{4a}. \tag{2.2.2}$$

Equations 2.2.1 and 2.2.2 for steady flow produce the pressure-flux rate relation shown in Figure 2f. It has the same shape as the HCW solutions and it is close to HCW with $T_n = 0.1$.

It is convenient to use the rescaled variables $q' = \dfrac{q}{4T_n}$, $p' = \dfrac{p}{4T_n}$, and $t' = T_n t$. (2.2.1) is the same and (2.2.2) becomes

$$\frac{da}{dt'} = -\frac{1}{1-a} + \frac{q'}{a}. \tag{2.2.3}$$

The fundamental objective of this study is to use (2.2.1) and (2.2.3) explore the dynamics with the three different upstream configurations sketched in Figure 2h-i. The first is a compressible storage reservoir lying upstream of the tube. The second is a fixed resistance in series with the tube fed by a reservoir at constant pressure. The third has multiple tubes connected by a manifold.

3. Compressible upstream

The addition of a compressible upstream reservoir can be considered to be a model of a magma delivery system in the earth, and possibly to planets and moons, too. Time-dependence is a fundamental feature of magma production in the earth irrespective of composition, temperature and geometry. Many mechanisms such as volatile content and outgassing, brittle behavior, viscosity variation, and crystal settling have been included in models, but this model produces time dependence without them. Additional features such as outgassing and viscosity variation might be added later to produce highly eruptive cycles with faster time scales (Wylie, et al. 1999b).

The simplest upstream condition consists of a reservoir of fluid with a free surface (essentially a compressible reservoir, Figure 2g) that is fed by a constant inflow q_u. (The prime is omitted here to be consistent with steady flow notation in section 3.1). Fluid flows out of the reservoir and into the tube with volume flux rate q'. The pressure change obeys

$$ {dp'}/{dt} = \tau(q_u - q') \quad . \tag{3.1} $$

The dimensionless growth rate is $\tau = \dfrac{\pi g S r_0^6}{8 A \nu \kappa L}$, where, g is acceleration of gravity, ν is kinematic viscosity, and L is length of the tube. It is the previous timescale scale (Stefan number $S = L_H / C_p(T_i - T_S)$ times r_0^2/κ) divided by a timescale for emptying an upstream reservoir of surface area A by viscous flow through the tube.

3.1 Stability with Compressible Upstream

Flow rate, radius and pressure is expanded into a zeroth order steady component and a time-dependent component

$$
\begin{aligned}
q' &= q_0 + \varepsilon q_1 \\
a &= a_0 + \epsilon a_1 \\
p' &= p_0 + \epsilon p_1
\end{aligned}
\qquad .
$$

Assume that the unsteady flow is smaller than the basic flow, $\epsilon \ll 1$. The O(1) steady solutions from 2.2.3 are

$$q_0 = \frac{a_0}{(1 - a_0)} = q_u. \tag{3.2}$$

thus
$$\alpha_0 = \frac{q_0}{q_0 + 1} \tag{3.3}$$

and from (2.2.1 for the primed values

$$p_0 = \frac{q_0}{a_0^4}, \tag{3.4}$$

thus
$$p_0 = {(q_0 + 1)^4}\big/{q_0^3} \quad . \tag{3.5}$$

The shape of (3.5) has the desired form shown in Figure 2f. The large asymptotic log-log slope corresponds to simple tube flow independent of T_n as in previous cases (Figure 2f). Minimum pressure is p_0=256/27=9.48 and this corresponds to the minimum at $q_0 = 3$ with radius $a_0 = \frac{3}{4}$. It has the same value of minimum pressure as approximately T_n =0.1 (from Figure 3 of Holmes (2007). The small asymptotic log-log slope of 2/1 has no counterpart in HCW.

The linear stability equations occur at order ε . Equation 2.2.1 leads to

$$q_1 = 4a_0^3 p_0 a_1 + a_0^4 p_1 \ , \tag{3.6}$$

(2.2.3) is

$$\left(\frac{d}{dt} + \frac{q_0}{a_0^2} + \frac{1}{(1 - a_0)^2}\right) a_1 = {q_1}/{a_0} \quad , \tag{3.7}$$

and (3.1) is

$$\left(\frac{d}{dt} + \tau a_0^4\right) p_1 = -4\tau p_0 a_0^3 a_1 . \tag{3.8}$$

These three are sufficient to calculate a growth rate. Substituting (3.6) in (3.7), using $q_0 = p_0 a_0^4$, and setting $a_1, p_1 \sim e^{\sigma t}$, (3.8) becomes

$$(\sigma + \tau\alpha_0^4)\left(\sigma - 3p_0 a_0^2 + \frac{1}{(1 - a_0)^2}\right) = -4\tau a_0^6 p_0 \tag{3.9}$$

with roots (using 3.2 and 3.5)

$$\sigma = \tfrac{1}{2}\left\{3p_0a_0^2 - \tau a_0^4 - \frac{1}{(1-a_0)^2} \pm \sqrt{\left(3p_0a_0^2 - \tau a_0^4 - \frac{1}{(1-a_0)^2}\right)^2 - \frac{4\tau a_0^3}{(1-a_0)^2}}\right\}. \tag{3.10}$$

The flow is unstable if growth rate σ has a positive real part. Because τ and a_0 are positive, the term $\frac{-4\tau a_0^3}{((1-a_0)^2)}$ is negative and the term under the radical sign has smaller real magnitude than the term to the left of the radical sign. Therefore, positive growth rate exists for

$$3p_0a_0^2 - \tau a_0^4 - \frac{1}{(1-a_0)^2} > 0. \tag{3.11}$$

At zero (neutral stability), (3.10) is imaginary and the flow oscillates but is overdamped for very small τ. Using (3.2-3.5), this can be rewritten as a function of either the upstream flux condition or of other steady flow properties. Defining

$$\tau_c = (3-q_u)(q_u+1)^6 q_u^{-5} \quad \text{or} \quad \tau_c = (3-q_0)p_0(q_0+1)^2 q_0^{-2} \tag{3.12a}$$

There is instability for

$$\tau < \tau_c. \tag{3.12b}$$

Curves for five values of τ_c are plotted in Figure 3a. Intersection progressively occurs further to the left with greater τ. Positive growth, which leads to instability and presumably ultimately freeze-up, lies to the left of the intersection and stability to the right.

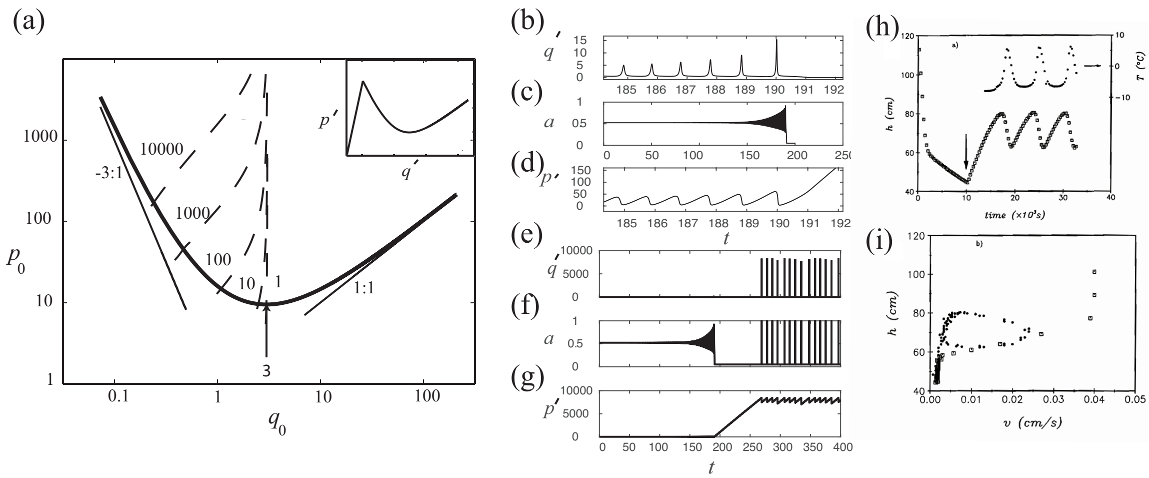

Figure 3. Results for compressible upstream. (a) Pressure-flux rate relation for steady flow (heavy curve (3.5)) along with small and large asymptotic logarithmic slopes for steady flow. Dashed curves are neutral stability (3.12a) for 5 different values of upstream compressibility rate τ. Inset, sketch of the curve with minimum radius added. (b) – (d) and (e) – (g) Flux rate, radius and pressure, for oscillating flow for q_u=1.1, $\tau = 100$ with a minimum radius of 0.05. (b) Flux rate during the short time interval when the minimum radius is reached by oscillating flow. (c) Radius over a longer time interval from the start until after the minimum radius is reached. (d) Pressure during the short time interval when the minimum radius is reached by oscillating flow. (e), (f), (g) The same records for an even longer time interval up to t=400 until after the second type of oscillation has developed. (h) Upstream elevation h (pressure) and temperature for viscous fluid flowing out of a cold tube with compressible upstream (Whitehead and Helfrich 1991). (i) Trajectory of h in phase space.

The curves are similar to those in Figure 6a of HCW. The limit $\tau_c = 0$ has pressure constant for all time and flow is stable for q_0>3. On the other hand, for $\tau \to \infty$ (very rapid response time) values of flux rate are stable and the entire curve is stable. These limits agree with those for the complete problem in Holmes (2007) and HCW.

3.2 Numerical results

Equations (2.2.1), (2.2.3) and (3.1) are easily integrated forward in time with finite differencing. Calculations over a wide range of many parameters verify the linear instability criteria with a typical example shown in (Figure 3b,c,d). The oscillation amplitude initially increases as in Figure 3c. At t=191.226, when amplitude becomes sufficiently large, there is an abrupt decrease in radius signifying a collapse to freeze up This starts at the instant when the smallest radius occurs in the cycle. Although this figure is typical, some cases can be highly damped with perturbations decaying exponentially from the beginning. In all cases the sudden decrease signifies freeze-up and radius plunges toward zero.

At the freezing stage in every one of our early numerical calculations, not only did radius plunge to zero, but also the calculation failed because (2.2.3) crossed zero, no matter how small the time step. At that point there were two options. One was to simply terminate the calculation and conclude freeze-up. This is fine in many instances, but in some cases, the calculation needed to continue. The second was to substitute a steady small *minimum radius* at every time step where radius is calculated to be negative or smaller than a fixed value. We found that this minimum radius always produces a small *seepage flow* that generates interesting new behavior without numerical failure. For the example in Figure 3c, the minimum radius was first invoked at t=191.226. After this, seepage flow continues and (3.1) leads to a gradual increase in pressure (Figure 3d,g) that occurs until flow rate is great enough for the seepage flow to melt back and open the tube following (2.2.3). In the model, the minimum radius adds an additional straight line in the pressure-flux rate curve from zero up to a point where it intersections (3.5) (see the inset, in Figure 3a). Then a new limit cycle oscillation occurs (Figure 3e,f,g) with pulses of rapid flow separated by very slow flow. Figure 3g shows that the upstream pressure during the limit cycle is much greater than the original pressure, and this is true for all oscillations throughout parameter space.

The period of the limit cycle depends on the minimum radius value, so in this sense, the minimum radius is now a property of the model. All aspects of the cycle are affected by minimum radius value including the time for build-up to the start of the limit cycle, the value of upstream pressure that is needed before the limit cycle begins, the limit cycle frequency, and the minimum and maximum values of flow rate and pressure for the limit cycle. The limit cycle involves a melt-back of the solid when pressure build up enough to make the seepage flow rapid enough. Surprisingly, this flow rate is less than the flow rate at the instant of the beginning of freeze up. This is apparently because the flow rate at melt back occurs when the linear flux versus pressure curve for the minimum radius intersects the far left end of the curve for steady flow as sketched in the inset in

Figure 3a. This aspect is noted also by Helfrich 1995 for flow focusing with temperature-dependent viscosity.

The cycles are similar to oscillations in tube flow with temperature-dependent viscosity and upstream compressibility (Figure 3h,i, from Whitehead and Helfrich 1991). There, instead of a minimum radius and seepage flow, there is the flow of a cold viscous "plug". This plug flow has a smooth p-q curve without discontinuous slopes like the cusp from the intersection of a straight line and (3.5) in our model, but both of them seem to produce the same behavior.

4. The dripping frozen faucet

4.1 Formulation

The second upstream condition imposed here has the configuration in Figure 2h. It is inspired by the very well-known flow of water in pipes and in natural springs that continues to persist during freezing temperatures. In fact, a common trick used by homeowners and plumbers to prevent pipe rupture during periods of freezing is to leave a water faucet with a the dripping rate that is quite small for small ranges of subfreezing temperature or short durations, the water in the pipe does not freeze shut. In another example of a similar process, water continues to flow out of rock fractures long after air temperatures fall to below freezing, resulting in large accumulations of ice. These can become hazards in subfreezing railroad and highway road cuts, with some of them reaching great size. A hint of why flow exists with below freezing temperature is found in the limit of large τ (Section 3) which is equivalent to an imposed steady flux rate where flow continues for any value (Epstein and Chueng, 1983, Holmes 2007, HCW). Therefore, an analysis of this problem that includes upstream dynamics of the dripping water pipe is useful.

First, the formula in the previous section 2.2.1 becomes

$$p' = \frac{q'}{a^4}. \tag{4.1}$$

Second, the upstream constriction, representing the valve in a faucet, can be pictured as a tube of radius r_f and length L_f. The scaled faucet pressure drop is thus

$$p'_f = \frac{q' r_0^4 L_f}{L r_f^4} \quad . \tag{4.2}$$

The freezing tube and the faucet (either upstream or downstream) are connected in series to a reservoir at fixed large upstream pressure p'_u so that

$$p' + Rq' = p'_u \quad . \tag{4.3}$$

This introduces the faucet resistance scale $R = r_0^4 L_f / r_f^4 L$. The value of critical resistance is R_c.

The other dimensionless equations are the same as in the preceding section and they are expanded as a power series about a steady flow. The steady flow occurs at the intersection of the basic steady flow (3.5) and the straight line for equation (4.3) (Figure 4b).

4.2 Stability

For stability, (3.6) and (3.7) for the first order perturbations are used along with

$$p_1 + Rq_1 = 0. \tag{4.4}$$

Setting $q_1, p_1 \sim e^{\sigma t}$, combining (3.6), (3.7) and (4.4), and then and using (3.2-5) to simplify the coefficients, the formula for growth rate is

$$\sigma = \left[\frac{(q_0+1)^3 \{(3-q_0)(q_0+1)^3 - R{q_0}^4\}}{q_0 \{(q_0+1)^4 + R{q_0}^4\}} \right]. \tag{4.5}$$

The sign of the perturbation does not matter. Because the slope of (3.5) is

$$dp_0/dq_0 = (q_0 - 3)(q_0+1)^3/q_0^4 \, , \tag{4.6}$$

growth rate is

$$\sigma = \left[\frac{(q_0+1)^3 \{-dp_0/dq_0 - R\}}{{q_0}^5 \{(q_0+1)^4 + R{q_0}^4\}} \right]. \tag{4.7}$$

Equation (4.7) has a simple physical interpretation. Simply start with the line $p_0 + Rq_0 = p_u$ at the zero flux axis whose intersection with (3.5) is indicated by the star in Figure 4a. Then, as p_u gradually decreases, pressure drop across the tube p_0 goes through the minimum at $q_0 = 3$ and then increases and remains stable until the slope $dp_0/dq_0 = -R$ is reached. This defines a critical resistance R_c, and a further decrease in p_u brings the line below the minimum. This has no solution and freeze-up must occur. If by some accident, a steady flow is started with p_u along with a flux rate q_0 intersecting the curve to the left of R_c, a positive perturbation (making total flux rate larger than the intersection point value) has a radius that grows and approaches the stable flow lying at the intersection on the right. Conversely, a negative perturbation has a negative perturbation to the radius that leads toward freeze up.

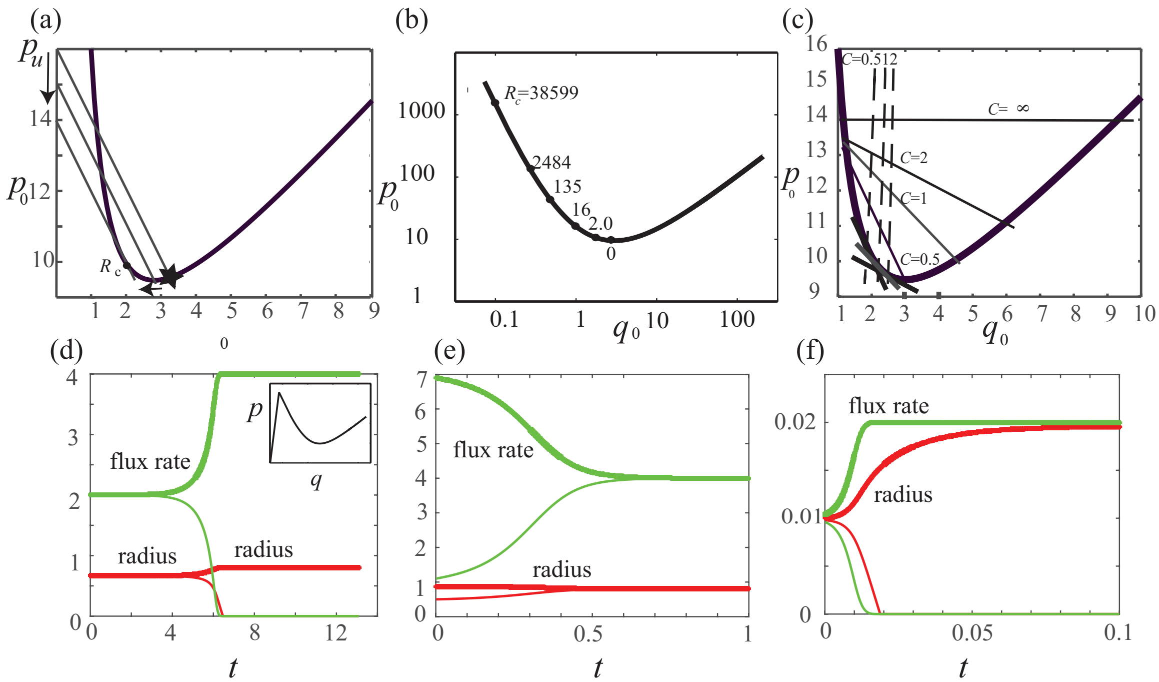

Figure 4. Results for two problems: for the faucet and two tubes. (a) A linear plot of three results with decreasing upstream pressure the for the faucet with *R=2*. The critical upstream pressure (tangential line) has a value of 14.11. (b) Some values of R_c for the faucet problem on a log-log plot. (c) Steady flows for two tubes with 4 values of *C*. The thin straight lines satisfy (5.6). The dashed curves are at the margins of (5.20) and instability growth is positive for any driving pressure greater than, or driving value of q less than those curves for each value of *C*. The short tangential lines show slope at minimum q_0. (d-f) Trajectories for numerical calculation with two tubes over time of a_1(thick red line), a_2 (thin red line), q'_1 (thick green line), and q'_2 (thin green line), for (d) q_u=2, *C*=1 with initial flux rate values close together progressing to seepage flow in one and full flow in the other. Inset, the three branch curve. (e) q_u=4, *C*=1, with very different initial flux rates, the two flux rates and both radii progress to equal values. (f) q_u=0.01, *C*=1 with initial flux rates close together progressing to seepage flow in one and full flow occupying the other.

Summarizing, stability is very sensitive to faucet radius and initial conditions. Freezing is readily prevented with a dripping faucet as long as *R* is small enough and flow is established. For example, a constriction with half the radius of the active tube has *R*=16. A freezing faucet might have an equivalent ratio of radii of tube/faucet much less than 10^{-2} resulting in *R*>O(10^8). Hence flow freezes up when the flow rate is reduced to a large negative slope on the left-hand branch. Freeze-up also occurs if the initial steady flow is small enough to lie to the left of (3.5)

5. Multiple tubes

Holmes (2007), numerically calculated flow in branching tubes where the source is comprised of a tube-manifold connected to a large number of tubes. The tube-manifold received uniform inflow along its entire length. The mathematical solutions were numerically stepped ahead in time to see the evolution of flows. Fifty identical tubes responded with influx values that should result in 6 or 7 active tubes with the rest freezing up. The calculations verified the expectation. It was necessary to set to zero the flux of any tubes that were freezing up and letting the pressure distribution along the manifold be determined by active tubes alone. Helfrich (1995) calculated planer flow with fluid having viscosity variation. This achieved flow focusing into discrete channels. Both results motivated the study of multiple tubes connected by a manifold.

5.1 Two Tubes—analytical results

Consider tubes each fed by a source with flux rate q_u with their upstream ends connected by a “manifold tube” that allows flow back and forth (Figure 2i). An upstream pressure condition is not imposed because it requires a different design. Starting with two tubes, the relations corresponding to primed (2.2.1) for tubes 1 and 2 are

$$p'_1 = q_1'/a_1^4, \qquad (5.1) \qquad\qquad p'_2 = q_2'/a_2^4. \qquad (5.2)$$

The equations corresponding to (2.2.3) are

$$\frac{da_1}{dt'} = -\frac{1}{1-a_1} + \frac{q'_1}{a_1}, \qquad (5.3) \qquad\qquad \frac{da_2}{dt'} = -\frac{1}{1-a_2} + \frac{q'_2}{a_2}, \qquad (5.4)$$

The manifold tube is kept at the upstream temperature and has different length and radius than the cooled tubes. Manifold flow resistance is inversely proportional to a resistance coefficient defined as $C=L\alpha_m^4/L_m r_0^4$ with α_m the dimensional radius of the manifold tube and L_m the physical length of the manifold tube. The two upstream conditions are

$$q'_1 + q'_2 = 2q_u, \qquad (5.5) \quad \text{and} \quad q'_1 - q'_2 = C(p'_2 - p'_1). \qquad (5.6)$$

Expanding as before, the equivalent equations to (3.2-4) are

$$p_{0i} = (q_{0i}+1)^4/q_{0i}^3, \qquad \text{with } i=1,2 \qquad (5.7)$$

and $$q_{0i} = \frac{a_{0i}}{1 - a_{0i}}, \tag{5.8}$$

so $$a_{0i} = \frac{q_{0i}}{q_{0i} + 1}, \tag{5.9}$$

and (5.3) and (5.4) require

$$q_{01} + q_{02} = 2q_u, \tag{5.10}$$

and $$q_{01} - q_{02} = C(p_{02} - p_{01}). \tag{5.11}$$

Obviously, two equal flows are possible so that $q_{01} = q_{02} = q_u$ and $p_{01} = p_{02}$. Another pair with steady flow rates exist with the intersections of (5.7) and the straight line (5.11). Four examples are shown Figure 4c. Intersections lie above the minimum $dp/dq = -C^{-1}$,

$$C = q_u^4/(q_u + 1)^3(3 - q_u), \tag{5.12}$$

which is equal to the inverse of (4.6). The limit of large *C* is a horizontal straight line with two steady solutions. This is obviously only valid for $q_u > 3$, since otherwise (5.10) is not satisfied. For finite *C*, the solution of (5.12) involves a fourth order polynomial with unknown analytical solutions. To supplement the analytical results, numerical results of (5.12) are easy to find and for *C*=1, for example, the minimum upstream flux rate allowing the solution is q_u=2.25208. (One can also expand the polynomial about the value 9/4 to find a close approximation to this). Therefore, for *C*=1 and q_u<2.25208, there is no intersection so that the only possibilities are either $q_{01} = q_{02}$ or unsteady flows. Although one might expect that a flow with small q_u would have a steady pair of rates with $q_{01} = 2q_u$ with virtually all of the flow exiting through one tube and with the other tube almost frozen up, this is impossible because flow rate for small flow produces an extremely large pressure drop that is too large to satisfy both (5.5) and (5.6) for fixed q_u. This problem is removed by adding another physical process, for example adding a *minimum radius* to allow seepage flow. This is done in all of the rest of our numerical calculations.

So far, the range of possible steady flows has been found , but are they stable? Let us denote the perturbation quantities by a curly overbar $\sim$. With steady flows, (equal or not) the equations governing small time dependent perturbations are first, the equivalents of (3.6) for each tube (*i*=1,2)

$$\tilde{q}_i = 4a_{0i}^3 p_{0i}\tilde{a}_i + a_{0i}^4 \tilde{p}_i \tag{5.13}$$

and second the equivalent to (3.7)

$$\frac{d\tilde{a}_i}{dt'} = \left[-\frac{1}{(1-a_{0\iota})^2} - \frac{q_{0i}}{a_{0\iota}^2}\right]\tilde{a}_i + \frac{\tilde{q}_i}{a_{0\iota}} \quad . \tag{5.14}$$

The conditions in the upstream tube connecting them are

$$\tilde{q}_1 + \tilde{q}_2 = 0 \quad , \tag{5.15}$$

$$\tilde{q}_1 - \tilde{q}_2 = C(\tilde{p}_2 - \tilde{p}_1). \tag{5.16}$$

It is convenient to modify (5.13) using the equivalent of (2.5) to eliminate a_{0i}

$$\tilde{p}_i = \frac{p_{0i}}{q_{0i}}\tilde{q}_i - \frac{4p_{0i}(q_{0i}+1)}{q_{0i}}a_i \tag{5.17}$$

For two equal flows, $p_{01} = p_{02}$ and using (5.16) to eliminate $\tilde{p}_i$ (5.17) becomes

$$(\tilde{q}_1 - \tilde{q}_2) = \frac{4\,p_{01}(q_{01}+1)}{C^{-1}q_{01} + p_{01}}(\tilde{a}_1 - \tilde{a}_2) \tag{5.18}$$

Using this with *i*=1,2 in (5.14) subtracted reduces to

$$\frac{d(\tilde{a}_1 - \tilde{a}_2)}{dt'} + \left[\frac{(q_{01}+1)^3}{q'_{01}} - \frac{4p_{01}(q_{01}+1)^2}{(C^{-1}q_{01}^2 + q_{0\iota}p_{01})}\right](\tilde{a}_1 - \tilde{a}_2) = 0. \tag{5.19}$$

The growth in radius difference is positive if the value within the square bracket is negative, which becomes, after some manipulation and setting $q_{01} = q_u$

$$p_{01} > \frac{q_u(q_u+1)}{C(3-q_u)} \tag{5.20}$$

Rewriting this using (5.7a), positive growth for instability requires

$$C > \frac{q_u^4}{(q_u+1)^3(3-q_u)} \quad , \tag{5.21}$$

which is identical to (5.12). The margins of both 5.12 and 5.21 for selected values of *C* are shown as dashed curves in Figure 4c and their intersection with the steady flow curve (bold) gives values of the critical flow rate that occurs exactly at the tangent to the curve. Therefore, for both two identical flows and the dripping faucet, the steady flow persists in the entire range where the upstream volume flux rate is large enough to satisfy the steady flow equations. For smaller flux rate, instability occurs.

5.2 Two tubes, numerical results

The numerical calculation advances the two values of a by one time step using (5.3) and (5.4) and then calculates q using these formulas derived from (5.1), (5.2) (5.5) and (5.6)

$$q_1 = \frac{2q_u a_1^4}{a_1^4 + a_2^4 + \frac{2}{C} a_1^4 a_2^4}\left[1 + \frac{a_2^4}{C}\right], \tag{5.22}$$

$$q_2 = \frac{2q_u a_2^4}{a_1^4 + a_2^4 + \frac{2}{C} a_1^4 a_2^4}\left[1 + \frac{a_1^4}{C}\right]. \tag{5.23}$$

Then, the new values determine both pressures at the new time. In practice, one tube might begin to freeze and end up with radius shrinking rapidly toward zero when seepage flow occurs. All calculations continue indefinitely as in section 3 by supplying an additional branch to the pressure-flux rate curve (See inset in Figure 4d) so that the curve bends down to zero for vanishing pressure and allows a small seepage flow. Comparison of runs with a minimum value of radius of 10^{-3}, 10^{-5} and even 10^{-13} gave the same results as the usual value that was used (10^{-4}). Therefore, the value of minimum radius does not determine stability. Three examples are shown in Figure 4d-f.

Numerical results over a wide number of parameters verify the analytic formulas in section 5.1. A run with q_u=2 is shown as an example. The criterion in (5.21) is $C<16/27$ for instability. With C=15/27, numerous calculations with a wide range of unequal starting amplitudes (ratios from 10^{-4} up to 10^{4}) had flows evolve to equal flow rates in both tubes like Figure 4d. Results not only confirm the linear stability prediction but the wide range of trial amplitudes indicates that the stability criterion is valid for all perturbation amplitudes (frequently described as globally stable). Figure 4e,f has examples for 2 other parameter pairs that approach balanced flows in one case and freeze-up in the other. Finally, in no case have two unequal flows like the straight line intersections in Figure 4c remained steady, but they always evolve to either two equal flows or one flow with freeze-up in the other. The only exception is if q_u is set to a value smaller than the value of seepage flow where both tubes acquire equal values of seepage flow.

5.3 Many Tubes- numerical results

Numerical calculations are easily formulated for more than 2 tubes. Each tube radius is advanced in time based on the radius and flux rate within each tube using equivalents of equations (5.3, and 5.4). Then, to calculate flux rate at the new radius, we consider first the pressure drop between for tubes *i* and *j*

$$q'_i - q'_j = C\left(p'_j - p'_i\right) \tag{5.24}$$

and this, along with the equivalent of (5.1) for every pair of tubes along the manifold, which are spaced $|i-j|$ apart becomes

$$q'_j = q'_i \frac{\left(1 + \dfrac{C}{a_i^4|i-j|}\right)}{\left(1 + \dfrac{C}{a_j^4|i-j|}\right)} = q'_i \frac{a_j^4(|i-j|a_i^4 + C)}{a_i^4|i-j|\left(a_j^4 + C\right)} \tag{5.25}$$

Then, one can use $\sum_{j=1}^{N} q'_j = Nq_u$ to express flux for the *i*-th tube

$$q'_i = \left\{\sum_{j=1}^{N} \frac{a_j^4(|i-j|a_i^4 + C)}{a_i^4\left(|i-j|a_j^4 + C\right)}\right\}^{-1} Nq_u \quad . \tag{5.26}$$

This resets flux rate for each tube after which the cycle is repeated.

To begin a numerical calculation, a fixed value of q_u and C is specified and the initial radius for tube number *i* has flux rate q_u(0.9995+0.0001var(i)) where var(i) is a random integer between zero and 10 from a numerical random number generator. Radii and flux rates in each tube thereafter advance in time until steady state is reached. When instability develops with some tubes having larger flows and others smaller ones, (5.26) proceeds without interruption even after seepage flow develops. When earlier attempts had no minimum radius equation, 5.26 developed shrinking denominators and instability occurred.

Figure (4a,b) shows a typical evolution of flux rate and radius for 101 tubes. Although the time step is small enough for different wavelengths of a perturbation to show different growth rates, as in the case of numerous stability problems as well as with temperature-dependent viscosity (Helfrich 1995, Wylie and Lister 1995). These calculations exhibited no selective wavelength. Instead, the random perturbation profile of both the flux rates and radii remains almost perfectly preserved during growth throughout an “early stage”. This stage terminates at different times depending on perturbation size, q_u and C. In this case it persisted up to t=0.3. Then, suddenly, from t=0.35 to 0.4 there is an “intermediate stage” where the profiles and radii have order one variation and they begin to dramatically change with some radii and flow rates plunging toward zero and others increasing. The evolution of some individual tubes is not easily understood. For example, a tube radius might first decrease and then increase or vice versa as the upstream manifold pressure distribution readjusts. Last, a late stage follows this until t=2, with some tubes approaching seepage and others fully flowing. Finally, all flux rates and radii in the active tubes become almost exactly equal and all seepage flux rates do too. A cross-manifold flow remains that distributes material from the uniform source to the active tubes. In this model, the ends of a manifold have zero lateral flux rate and this exerts some influence not yet documented or understood. In spite of this, results are clear. For example, the steady final distribution at t=2 for q_u=0.1, C=1 results in flow in 6 tubes (Figure 5a). A sequence with an unchanging distribution in the early stages of a numerical model with viscosity variation of cylindrical-slab flow seems to be similar to this (Figure 14 of Helfrich 1995). That run ends up with one flowing region and everything else decaying away just like our results for the limit of small flux rate.

Our small minimum radius value of 0.0001 used for these figures makes reproducible results (subject of course to the limits of random initial conditions). The seepage flux rate is completely negligible in the volume flux budget at the end of all calculations. For example, even for the extreme case with 10^4 tubes where only one tube remains active at the end of the freezing up sequence, less than 1% of the imposed flux goes through the 999 seeping tubes.

This evolution of small perturbations that grow and results in flow that becomes equal in selected tubes occurs in every case of our 1183 numerical runs with results spanning wide ranges of q_u (10^{-5} – 100), C (10^{-4} – 10^8) and N (2 to 10000) (listed in Supplementary Tables). Each realization follows the nonlinear evolution ending in a few actively flowing tubes with equal flux rates (Figure 5a) and radii (Figure 5b). A variation of the spacing away from the center exists, but such an effect only becomes large (more than tens of percent) for N>1000. The number of final tubes, #, has a statistical spread in 1000 realizations (Figure 5c). The distribution is insufficient to determine whether it is bell shaped, which might not happen because of the nonlinear evolution.

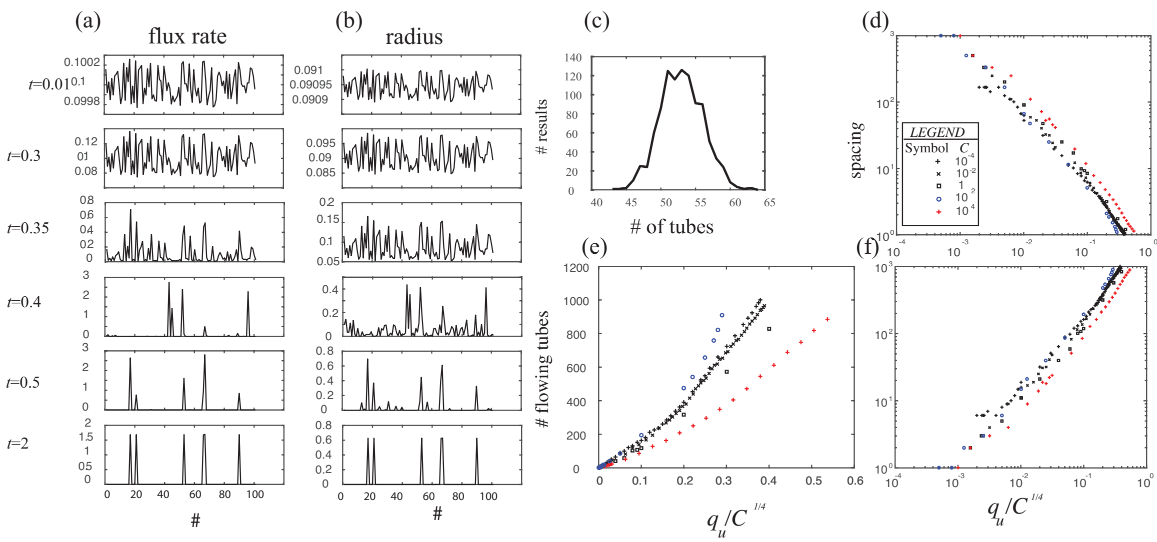

Figure 5 (a) Flux rate and (b) radius at various times starting from random initial conditions (q_u=0.1, C=1, N=101). The first two times are during "early evolution" when the distribution profile is amplified without change of shape. The next two times are during "middle evolution" when the profiles change because some of the radii become much smaller and each flux rate either grows or decays. The bottom two times are during "final evolution" when flowing and seepage tubes become fixed. The 6 flowing tubes end with equal rates and radii with all other flux rates and radii shrunk to negligible size. (c) The number of actively flowing tubes for 1000 different runs (q_u=0.05, C=1, N=1000). (d) The spacing of tubes N/# versus $q_u/C^{1/4}$ (logarithmic) with a legend of symbols for values of C. (e (linear) and f (logarithmic) number # of flowing tubes.

After flow is steady, all the flowing tubes have almost exactly the same flux rates and radii so they arrive at one point on the p-q curve. No known rule exists for the final rate location. For example, the rate in Figure 5a is about q=1.7 which is less than the minimum q=3 (Figure 3) and lies on the unstable branch. Therefore, the concept of "some flows are in the stable branch and others decay on the unstable branch" does not hold. Perhaps others will think, as I did, that this is surprising, but Helfrich (1995) also reports that numerical results of flows with fingering due to temperature-dependent viscosity do not cluster to the stable branch.

After some searching, a systematic dependence between tube number # (consequently spacing N/#), and the parameter group $q_u/C^{1/4}$ was found for wide ranges of C (10^8) and q_u ($1.5\text{x}10^4$). All tubes support flowing for $q_u/C^{1/4}>0.55$ and flow fills fewer tubes for the remaining 154 runs. The trends in log-log space are remarkably linear, parallel and logarithmically close to linearly proportional to $q_u/C^{1/4}$ (Figure 5b,d) in spite of no averaging as in Figure 5c for randomness.

Since C is proportional to the fourth power of the radius of the manifold tube a_m, $C^{1/4}$ will be called the "scaled manifold radius". The linear trends in Figure 5d,f have a slope proportional to $\left(q_u/C^{\frac{1}{4}}\right)^{-1}$ so active tube spacing N/# is linearly proportional to scaled manifold radius. To quantify the results further it is useful to note that the flux rates in each active tube are equal (e. g. Figure 5a,b at t=2) so each rate is simply $q=Nq_u/\#$. All radii are also equal so that the radius a for steady flow in each active tube is readily calculated using equation (3.3). The ratios of this radius compared to the scaled manifold radius $a/C^{1/4}$ for the points shown in Figure 5 are shown in Figure 6a. The ratios are not constant, but they all are clearly of order one. For $C \leq 1$ the ratio $a/C^{1/4}$ has considerable variation of a little over 2 with a total range from 0.3 to 0.68. For C=100, the mean ratio is 0.225 with a standard deviation of 0.003. For C=10^4, the mean ratio is 0.082 with standard deviation 0.0088. Therefore, to a first approximation the radius within a flowing tube is linearly proportional to the scaled manifold radius $C^{1/4}$ with a proportionality constant (Figure 6a) that is order one.

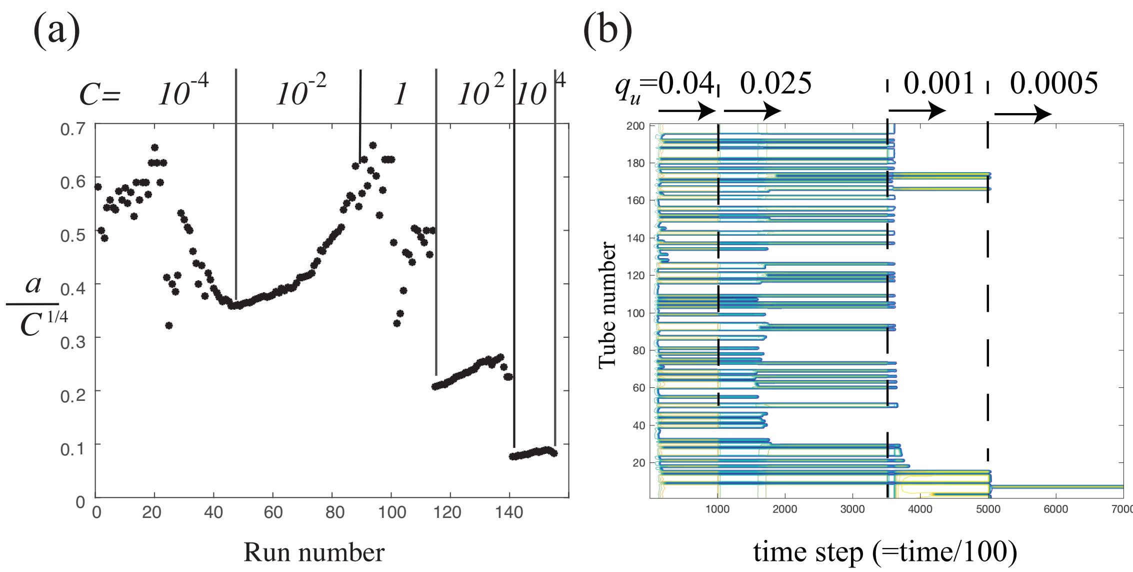

Figure 6. (a) Radius within each flowing tube after a reasonably steady flow is achieved divided by the scaled manifold radius. The numbered runs occupy a wide range of q_u (Figure 5). (b) Evolution of

the contours of tube radius for a 200 tube manifold with sequentially decreased flow rates for C=0.0001. The sequential values of # are 97, 67, 5 and 1.

Figure 6b shows contours of radius for all active tubes with 4 progressively lower values of q_u, and is a good illustration of the spacing of active tubes. When this run is continued with the opposite sequential increases in q_u there is hysteresis with no increase in the number of active tubes. This is explained by considering that for flow in a single tube, the total flux rate is 0.04x200=8 making an upstream pressure of about 12 (see Figure 4a). This pressure makes only a tiny seepage flux rate of 1.2×10^{-15} but the seepage flux rate needed for the straight line of seepage flow to intersect equation (3.5) is over 1.

What might these results imply for the spacing of outflows in nature? Let us try first to look at the formation of vents along a volcanic fissure. The number of tubes for N=1000 in Figure 5 is roughly fit by the relation

$$\#=800 q_u C^{-1/4} \qquad (5.27)$$

Make a model of a fissure composed of 10^3 tubes spaced L_m=10 m apart feeding melt up from a shallow reservoir at a depth L=1000 m below the surface. A total flux of Q=1 m^3s^{-1} is evenly distributed at 1000 m depth and therefore the flux per tube is Q=0.001 m^3s^{-1}. Using $q_u = Q/\pi^2\kappa L T_n$ along with magma thermal diffusivity $\kappa=5\times10^{-7}$ m^2 s^{-1}, and T_n=10, gives q_u=0.020. As a first guess equating the radius of the manifold tube to the tube to the surface so that $r_o=r_m$ and $C=L/L_m$ then (5.27) gives that $\#=16/10^{1/2}=5$ tubes that are active over the 10 km extent so there is a vent every 2 km. With greater depth of the fissure and everything else the same, then q_u is smaller and there are fewer active tubes with wider vent spacing. These distances are plausible and given the great differences between this simple model and complex reality, the test seems to be promising.

Let us try a second example-- the general problem of magma focusing at mid-ocean spreading centers. Pretend that there is a manifold consisting of a continuous mushy zone along a 1000 km long ridge with vertical tubes each spaced 1 km apart that might bring melt up to the surface. To pick flux rate, we need to produce a flux that generates an oceanic crust thickness of 7 km with a ridge with a moderate spreading rate of 0.1 m y^{-1} (=3.2×10^{-9} m s^{-1}). This gives a flux rate per tube spaced over the 1 km width covered by each tube of approximately 0.022 m^3s^{-1}. Using a value of L=30 km, (a minimum value for the depth), the same values of thermal diffusivity and T_n as above, then the dimensionless value of flux rate is q_u=0.0149. There is little knowledge of what the equivalent for r_m would be for either mushy zones or magma chambers under the ocean floor, so for a crude start use C=1. (Note that a new model with a porous manifold is quite feasible.) This gives 12 active tubes for the ridge, equivalent to spacing of 83 km. This exceeds the spacing that is more typically 20-40 km for moderate rate mid-ocean spreading centers. Note also that this calculation implies that spacing is inversely proportional to flux rate so that with the present parameters ultra-slow spreading centers might have spacings over 100 km and the fastest might have spacing less than 50 km.

Therefore, the results show that magma cannot rise up everywhere in fissures and spreading centers and there are presumably ranges of parameters where volcanic intrusions might even freeze shut. Note that the volume flux rate used here is equal to 0.7 km^3/y for the 1000 km ridge, which reduces to a volume flux rate for each of the 12 tubes of 0.058 km^3/y which is in the middle of the range of active volcanos in White et al. (2006). They present other considerations that ours for the thermal cooling of the chambers as suggested constraints on the size of the volcanos. There are many other suggested dynamical factors governing the spacing of volcanos. To name a very few, there is Rayleigh-Taylor buoyancy that involves viscosity of the mushy zone (Schouten et al. 1985), there are combined buoyant, tectonic and mantle-forced flows (Magde and Sparks 1997), and there is even deeper mantle flow (Vanderbrock et al, 2016 and references therein). Results of this simple model suggest that lateral migration in the mushy zone with rising modulated by localized freezing dynamics might also be important and these dynamics can be added to the existing list.

In summary, the model curve in Figure 3a is incomplete for many models because freezing builds up impossible pressure in the manifold. The imposition of a minimum radius (Figure 3a inset) removes this inadequacy. With it, both a limit cycle for compressible upstream and multiple tubes up to $N \leq 1000$ work well at documenting evolution of flow. For $q_u/C^{1/4}$<0.55 both the spacing between active tubes and the value of the active tube radius depends primarily on the scaled manifold radius $C^{1/4}$. For growth from random noise, the relation between q_u and # is not unique. Statistical results end up clustering around a central peak to give # and the spacing. Finally, the results seem to be in crude accord with the spacing of magmatic centers in mid-ocean ridges.

6. Discussion

This simple model is used to analyze a number of flows with different upstream conditions. Explicit formulas lead to insight into freezing dynamics for each upstream condition with formulas for stability and other aspects of each flow. For a compressible upstream chamber, the two limits of constant pressure and constant flux rate are recovered and results are similar to those by Holmes 2007 and HCW. For the frozen water faucet configuration, freeze-up occurs when the pressure change of the flow equals slope of the curve in Figure 4. For branching tubes, (5.21) indicates that freeze-up of one of a pair of tubes occurs if the inverse of the resistance coefficient between the two tubes upstream is greater than the tangential slope for that coefficient in Figure 4. For all three configurations, numerical calculation with finite time steps cannot extend all the way to perfect freezing unless one develops a special numerical method to remove high pressures for very small flow with very small radius for long times. We resort to a minimum radius that allows numerical integration to proceed to final flows.

The compressible model is intended to be the simplest possible model of a time-dependent magma delivery system. It omits variations in volatiles and viscosity, but it has the three important elements listed below.

1. There is a single reservoir driven by a steady influx of material. The reservoir accumulates pressure to drive the melt upward through the colder surface of the earth. The reservoir in this model is linearly compressible, but that compressibility is meant to replace all the effects of buoyancy force driven by the density difference between magma and rock as well as the excess pressure from the elastic surroundings as magma accumulates under the region.

2. There is a permanent pathway to the surface, represented here by a simple cold tube with the added feature that it allows seepage flow. The pathway in our model represents both cracks from stress in the elastic plate that are abundantly observed seismically, brittle and weak material in the pathway and preheated aseismic pathways that guide magma ascent. There is a minimum of different structures along the flow and storage paths and no mechanical opening of a crack.

3. The melt can solidify along the tube . There are no volatiles, flow is one-dimensional with composition and viscosity constant, and most important the model eruption cannot happen unless the outflow is rapid enough to melt back the solid sheath of the tube. (like the melt-back of a fissure as in Bruce and Huppert 1989).

The dynamics of the spacing of active tubes and the relation between spacing and the scaled manifold radius $C^{-1/4}$ is obviously caused by the relatively close correlation between active flowing tube radius and scaled manifold radius although there is also a weak influence by C.

Although flow and freeze-up with true solidification differs from flow with viscosity variation, we found that invoking a minimum radius makes solidifying flows very similar to flow of fluids with large temperature-dependent viscosity. For example, when our *minimum radius* is inserted, there is a branch of the pressure curve that bends down to zero as flow approaches zero (Figure 3a inset), just like flows with temperature-dependent viscosity (Whitehead and Helfrich 1991, Helfrich 1995, Wylie and Lister 1995, and Wylie et al. 1999a). Possibly the model of Wylie and Lister (1995) with a step change in viscosity is the closest equivalent to our solidification model, although that does not include a latent heat of fusion. In any case, the flow with variable viscosity inherently has seepage flow so that our new results seem to apply to such problems. Although a systematic investigation of hysteresis in this problem might be interesting, it can be more usefully conducted for the problem of viscosity variation rather than freezing since the minimum radius is added to this model.

The *minimum radius* allows a tube to recover from seepage when upstream pressure becomes large enough. The reason why a minimum radius is required for all time in both sections 3 and 5 is fundamental if one wants to avoid the discontinuity of freeze-up. For section 3, the flow rate-pressure curve must have two extrema so that 3 possible intersections with a straight line exist rather than the 2 intersections in Figures 3 and 4. In that way, two intersections are stable and the third middle one is not, so oscillations can come to equilibrium. In section 5, the minimum radius prevents excessively large pressures that are associated with very small flow rates and radii.

Perhaps other physical processes instead of a minimum radius can be invoked numerically for solidifying flows. In any event, the need to invoke a minimum radius makes the results with large viscosity variation and with solidification very similar so future projects might simply use one or the other, depending on which is most convenient. In addition, some numerical results in section 3 clearly apply to flow with viscosity variation and this should also be true for section 5.

There are innumerable interesting extensions. One can combine these upstream conditions to flows with both viscosity variation and solidification, or have a slightly porous solid, or incorporate non-Newtonian flows like those reviewed by Kavanagh et al. (2018), or make a model of sedimentation problems or extend this approach to more complex flow geometry. It is not difficult to imagine the occurrence of very complicated or even truly chaotic flows. With enough complications, even realistic random-appearing patterns (Klein 1982) could probably be generated. It is hoped, however, that the interesting behavior of these models with relatively simple flow situations can start to explain some of the elaborate piles of material that are encountered in igneous, frozen and depositional structures in the earth.

Acknowledgments: Emeritus funds are provided by Woods Hole Oceanographic Institution. All data are shown in the supplementary tables or can be measured in the Figures. No external repository exists.

References

Björnsson, H. (1998). Hydrological characteristics of the drainage system beneath a surging glacier *Nature* 395, 771-774 | doi:10.1038/27384.

Bruce, P. M. & Huppert, H. E. (1989). Thermal control of basaltic fissure eruptions. *Nature* 342, 665–667.

Bruce, P. M. & Huppert and H. E. (1990). Solidification and melting in dykes by the laminar flow of basaltic magma, in *Magma Transport and Storage*, M. P. Ryan, Ed. Pp. 87–102. Wiley, New York, 420 pp.

Chadam, J., Hoff, D., Ortoleva P. & Sen, A. (1986) Reactive-infiltration instability, *J. Appl. Math.,* 36, 207-238.

Daccord, G. (1987) Chemical dissolution of a porous medium by a reactive fluid, *Phys.*

Rev. Lett., 58, 479-482.

Dragoni, M., Donza, F. and Tallarico A. (2002). Temperature distribution inside and around a lava tube. *Journal of Volcanology and Geothermal Research* 115, 43–51.

Epstein, M. & Chueng, F. G. (1983). Complex freezing-melting interfaces in fluid flow *Ann. Rev. Fluid Mech. 15*, 293.

Graetz, L. (1883), Uber die Wärmeleitungsfähigkeit von Flüssigkeiten, *Annalen der Physik und Chemie* 18, 79

Helfrich K. R. (1995) Thermo-viscous fingering of flow in a thin gap: a model of magma flow in dikes and fissures. *J Fluid Mech.* 305, 219–238.

Hirata, T. & Ishihara M. (1985) Freeze-off conditions of a pipe containing a flow of water, *Int. J Heat Mass. Trans.* 28, 331-337.

Holmes, M. (2007) Length and shape of a lava tube, in: *Woods Hole Oceanographic Institution Geophysical Fluid Dynamics Program Proceedings*. http://www.whoi.edu/page.do?pid=19276.

Holmes-Cerfon, M. C. & Whitehead, J. A. (2011). Instability and freezing in a solidifying melt conduit, *Physica D*, 240, 131-139.

Kavanagh, J. L., Engwell, S. L., & Martin, S. A. (2018) *Solid Earth,* 9, 531–571, https://doi.org/10.5194/se-9-531-2018

Kelemen, P., Whitehead J. A., Aharonov, E. and Jordahl K., (1995). Experiments in flow focussing in soluble Porous Media, with Applications to Melt Extraction from the Mantle *J. Geophys. Res.* 100, 475-96.

Klingelhofer, F., Hort, M., Kumpel, H. J., & Schmincke, H. U. (1999). Constraints on the formation of submarine lava flows from numerical model calculations.

Klein, F. W. (1982) Patterns of Historical Eruptions at Hawaiian Volcanos, *J. Volcanology and Geoth.l Res.* 92, 215–229.

Magde L. A. and Sparks, D. W. (1997) Three-dimensional mantle upwelling, melt generation, and melt migration beneath segment slow spreading ridges J. Geophys Res. – Solid Earth102, 20571-20583

Mulligan, J. C. & Jones, D. D. (1976). Experiments on heat transfer and pressure drop in a horizontal tube with internal solidification. *Int. J. Heat and Mass Transfer* 19, 213-219.

Pansino, S., Emadzadeh, A., & Taisne, B. (2019). Dike channelization and solidification: Time scale controls on the geometry and placement of magma migration pathways. *Journal of Geophysical Research: Solid Earth,* 124, 9580–9599. https://doi.org/10.10292019JB018191

Richardson, S. M. (1983). Injection moulding of thermoplastics: Freezing during mould filling**.** *Rheol. Acta* 22, 223-236.

Richardson, S. M (1985). Injection moulding of thermoplastics: 1. Freezing-off at gates, *Rheol. Acta*, 24, 497-508.

Richardson, S. M. (1986). Injection moulding of thermoplastics: Freezing of variable-viscosity fluids. III Fully developed flows, *Rheol. Acta*, 25, 372-379.

Rubin, A. M. (1993). On the thermal viability of dikes leaving magma chambers. *Geophysical Research Letters,* 20, 257–260. https://doi.org/10.1029/92GL02783

Sakimoto, S. E. H., & Gregg T. K. P. (2001). Channeled flow: Analytic solutions, laboratory experiments, and applications to lava flows. *J. Geophys. Res.* 106, 8629-8644.

Sakimoto, S. E. H. & Zuber, M. (1998). Flow and Convective cooling in lava tubes. *J. Geophys. Res.* 103, 27465-27487.

Taisne, B., & Tait, S. (2011). Effect of solidification on a propagating dike. *J. Geophys. Res.,* 116, B01206. https://doi.org/10.1029/2009JB007058

Taisne, B., Tait, S., & Jaupart, C. (2011). Conditions for the arrest of a vertical propagating dyke. *Bull. Volcanology*, 73, 191–204. https://doi.org/10.1007/s00445-010-0440-1

VanderBeek, B., Toomey, D., Hooft, E. *et al.* Segmentation of mid-ocean ridges attributed to oblique mantle divergence. *Nature Geosci* **9,** 636–642 (2016). https://doi.org/10.1038/ngeo2745.

Weigand, B., Braun, J., Neumann, S. O & Rinck, K. J. (1997) Freezing in forced convection flows inside ducts: a review, *Heat Mass Transfer* 32, 341–351.

White, S. M. Crisp, J. A. and Spera, F. J. Long-term volumetric eruption rates and magma budgets, Geochem. Geophys. Geosystems, 7,3, Q03010, doi:10.1029/2005GC001002.

Whitehead, J. A., & Helfrich, K. R. (1991) Instability of flow with temperature-dependent viscosity: a model of magma dynamics. *J. Geophys Res* 96,4145–4155.

Wylie, J. J., & Lister, J. R. (1995) The effects of temperature-dependent viscosity on flow in a cooled channel with application to basaltic fissure eruptions. *J Fluid Mech* 305, 239–261.

Wylie, J. J., Helfrich K. R., Dade B., Lister, & J. R. Salzig, J. F. (1999a) Flow localization in fissure eruptions. *Bull. Volcanol.* 60 , 432–440.

Wylie, J. J., Voight, B. & Whitehead, J. A. (1999b) Instability of magma flow from volatile-dependent viscosity, Science 285, 1883-1885.

Zerkle, R. D. and Sunderland, J. E. (1968), The effect of liquid solidification in a tube upon laminar-flow heat transfer and pressure drop. *J. Heat Transfer, Trans*. ASME Series C , 90, 183-190.